Portugaliae Electrochimica Acta 2010, 28(2), 135-142

DOI: 10.4152/pea.201002135

PORTUGALIAE ELECTROCHIMICA ACTA
ISSN 1647-1571

Electrochemical Evaluation of Wrought Titanium –15 Molybdenum Alloy for Dental Implant Applications in Phosphate Buffer Saline

Rahul Bhola,[*] Shaily M. Bhola, Brajendra Mishra, David L. Olson

Department of Metallurgical and Materials Engineering, Colorado School of Mines, Golden, CO, USA

Received 20 July 2009; accepted 12 April 2010

Abstract

Ti-15Mo alloy has been evaluated for its electrochemical behavior in phosphate buffer saline solution at the physiological temperature of 37 ºC. A two time constant model of a duplex oxide layer has been used to assess the corrosion behavior of the Ti-15Mo alloy-solution interface using electrochemical impedance spectroscopy (EIS). Interfacial characteristics of the inner barrier layer and the outer porous layer have been studied to understand the role of the alloy as an implant. Ti-15Mo alloy shows a very high barrier layer resistance and a tendency to resist localized corrosion.

Keywords*:* titanium, implant, impedance, β-alloy, phosphate buffer saline.

Introduction

Titanium and its alloys are widely used in odontological applications due to their high corrosion resistance, mechanical properties and biological stability in the stomatognathic environment [1]. Ti-6Al-4V alloy with α+β hybrid microstructure was the first titanium alloy used as an implant material because of its high strength, low elastic modulus, high corrosion resistance and tissue tolerance [2-4]. However, studies have shown that the leaching of aluminum and vanadium after a threshold may cause peripheral neuritis, osteo-malacia, hypersensitivity and Alzheimer's diseases [5-7]. There has been, therefore, an increasing interest over the last decade to develop alloys without aluminum and vanadium. Moreover, stabilizing the metal matrix with β stabilizing alloying elements such as molybdenum, niobium, tantalum, zirconium improves strength and lowers the

[*] Corresponding author. E-mail address: rbhola@mymail.mines.edu

modulus mismatch between the implant and the bone, thereby promoting higher osteo-integration and implant performance [2-3,8-13].
Ti-15Mo alloy is a metastable beta alloy whose basic metallurgy, mechanical and corrosion resistance properties have been thoroughly described in the metallurgical literature, especially its biocompatible advantages [14-17]. Ti-15Mo alloy has a beta (body centered cubic crystal structure) phase stability with higher strength than alpha and alpha-beta dual phase alloys and a lower modulus of elasticity and lower stiffness which is beneficial for orthopaedic/dental applications. The production flow sheet for the Ti-15Mo high strength rods has been described by Davis et al.[18]. This alloy has its own ASTM designation [19].
The aim of this paper is to evaluate the electrochemical behavior of Ti-15Mo alloy in phosphate buffer saline solution at the physiological temperature of 37 ºC.

Experimental

Materials preparation

The basic metallurgy, mechanical and corrosion resistance properties for Ti-15Mo alloy has been thoroughly described in the metallurgical literature, especially its biocompatible advantages [14-17]. Ti-15Mo alloy has a beta (body centered cubic crystal structure) phase stability with higher strength than alpha and alpha-beta dual phase alloys and a lower modulus of elasticity and lower stiffness which is beneficial for orthopaedic/dental applications. The production flow sheet for the Ti-15Mo high strength rods has been described by Davis et al. [18]. The microstructure for this alloy is given in Fig. 1. This alloy has its own ASTM designation [19].

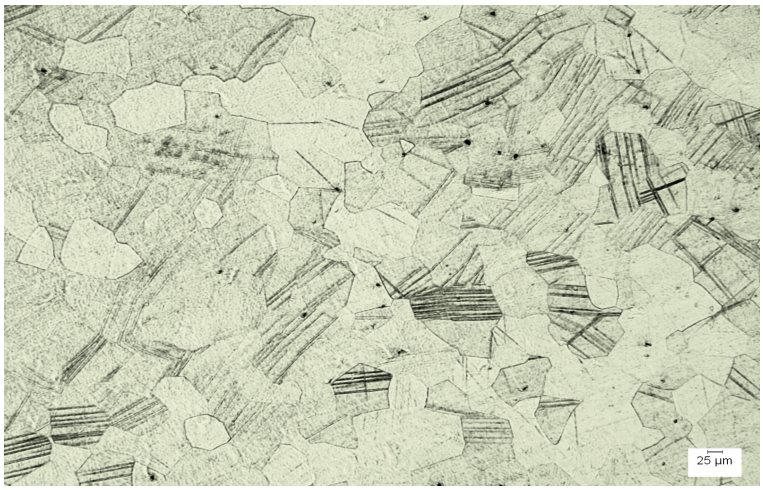

Figure 1. Equi-axed β-structure for Ti-15Mo (BCC).

Ti-15Mo titanium alloy (UNS R58150)[19] of composition 0.05%C, 0.1%Fe, 0.015%H, 0.01%N, 0.15%O, 15%Mo and 84.67%Ti (wt.pct) was used for the present investigation. Available cylindrical rods were cut to expose cross section area of 0.4869 cm^2 for immersion. The specimens were then joined at one end

with a copper wire using a conducting silver epoxy and left overnight to dry. The coated samples were mounted in an epoxy resin, leaving the base exposed for corrosion studies. The exposed surface of the specimens was finished with different grades of silicon carbide grit papers (up to 2400 grit) and polished using a diamond abrasive wheel to quarter micron finish, washed with double distilled water and acetone.
Phosphate buffer saline solution of pH 7.4 and composition 0.137 M sodium chloride, 0.0027 M potassium chloride and 0.01 M phosphate buffer was used to carry out the electrochemical testing for the Ti-15Mo alloy.

Measurements
The following measurements were performed on Ti-15Mo alloy in phosphate buffer saline solution at the physiological temperature of 37 ºC. A three-electrode cell assembly consisting of titanium alloy as the working electrode, platinum wire as the counter electrode and a saturated calomel electrode as the reference electrode was used. The DC electrochemical measurements were conducted using a PAR Potentiostat 273A and for AC impedance measurements, a PAR 1255 FRA was used.

Microstructure
The metal specimens were degreased, dried and mounted in bakelite resin. Mechanical grinding was done with SiC papers on a water cooled grinding stage upto paper 1800. Polishing was performed using gradually decreasing sizes of diamond abrasive from 6μ to 1μ and finally using a fine grained Al_2O_3 (with decreasing particle size from 0.5μ to 0.25μ) and cold saturated hydrous oxalic acid suspension on a short circular velvet cloth. The specimens were washed in de-ionized water and ethanol and air dried before etching. A universal etchant commonly known as the Kroll's reagent, a hydrous solution comprising of 2 ml HF (40% conc.) and 6 ml HNO_3 (65% conc.) in 100 ml H_2O (de-ionized) was used for etching. The microstructure obtained was determined using optical microscopy and has been shown in Fig. 1.

Electrochemical Impedance Spectroscopy (EIS)
Impedance measurements were performed on the system at an open circuit potential for various intervals up to 360 hours. The frequency sweep was applied from 10^5 to 10^{-2} Hz with the AC amplitude of 10 mV.

Cyclic Potentiodynamic Polarization
Cyclic polarization measurements were performed by polarizing each electrode from -250 mV versus the open circuit potential up to the vertex potential of 2 V versus the reference electrode, after which the scan was reversed and the final potential was the same as initial potential, that is, -250 mV as a function of the open circuit potential. The ASTM standard scan rate of 1 mV/s was used for the polarization sweep [20].

Results and discussion

The microstructure for Ti-15Mo alloy as shown in Fig. 1 primarily consists of large equiaxed grains of the β phase. Only a very small volume fraction of grain boundary α phase is present in the microstructure. The α laths formed during alloy aging nucleate within the interior of the grains and along the grain boundaries and are visible at higher magnifications. Growth and annealing twins are also visble in the micrograph.

Fig. 2 shows the equivalent circuit that was used to fit the impedance results. Many circuit models were tried, but the closest fit with least chi-square value was obtained with the circuit shown. This circuit is based on the duplex structure of the oxide formed in solution on the surface of Ti-15Mo, composed of an inner barrier layer and an outer porous layer. The barrier layer is compact, having a high resistance, whereas, the outer layer is porous. R_s, R_p and R_b represent the solution, porous layer and barrier layer resistance, respectively. CPE_p and CPE_b are the capacitances of the porous layer and the barrier layer, which are represented by a constant phase elements. W_b represents the Warburg element for the barrier layer, accounting for the Warburg impedance, Z_W. Warburg impedance is used as a circuit element for a diffusion controlled process and is characterized by three parameters, W(R), W(T) and W(P). W(R) indicates the length of Z_W, W(T) is the length of effective diffusion and W(P) is related to the slope value such that $0 < W(P) < 1$.

Similar studies in literature have revealed the presence of a bilayer oxide formed over titanium alloys. Badawy et al. [21] have proposed a two time constant circuit for the corrosion behavior of porous titania films on titanium in PBS solution where the two time constant represents the barrier and porous layers of the duplex passive film. Al-Mayouf et al. [22-25] have also reported the duplex oxide structure for a titanium alloy in artificial saliva.

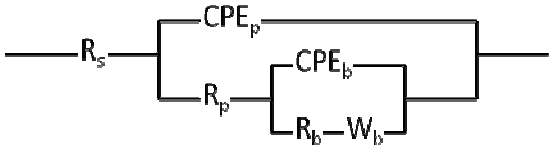

Figure 2. Equivalent electric circuit used to simulate titanium alloy-PBS interface.

Figs. 3 and 4 show the Bode and Nyquist plots for different immersion times of Ti-15Mo alloy in PBS solution at 37 ºC. The nature of the alloy-solution interface does not change with immersion time as can be seen from these figures. At all immersion times, the system fits into the same circuit model. Various electrochemical impedance circuit elements, calculated using the circuit in Fig. 2, are shown in Table 1. Value of n for the porous layer capacitance is close to 1, suggesting that the porous layer is close to a perfect capacitor. On the other hand, the value of n for the barrier layer capacitance is around 0.5 or 0.6, which is due to diffusion and hence a Warburg element is included to account for the same. As seen in Table 1, $W_b(R)$ value decreases with immersion time and reaches an almost constant value.

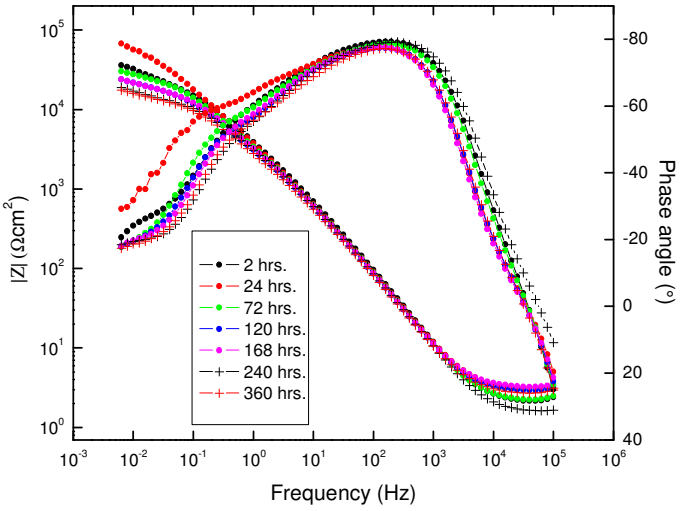

Figure 3. Bode plot for Ti-15Mo alloy in PBS solution at 37 ºC.

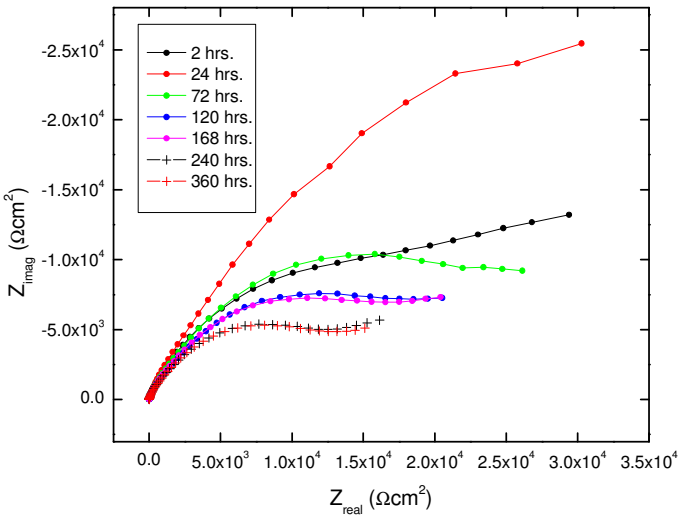

Figure 4. Nyquist plot for Ti-15Mo alloy in PBS solution at 37 ºC.

The capacitance of the inner barrier layer shows an overall increase up to 360 hours whereas the capacitance of the outer porous layer does not follow a trend and does not increase or decrease markedly. The barrier layer resistance is an order of magnitude higher than the porous layer resistance. The barrier resistance increases till 24 hours of immersion and then slowly falls till 360 hours of immersion. On the other hand, the porous layer resistance does not follow any specific trend, which may be due to the changing characteristics of the porous layer caused to the incorporation of ions into the pores from the solution. It has been suggested that the hydrated phosphate ions are adsorbed on a hydrated titanium oxide with the release of water as:

$$Ti(OH)_{(ox)}^{3+} + H_2PO_{4(aq)}^{-} \rightarrow Ti_{(ox)}^{4+}HPO_{4(ads)}^{2-} + H_2O$$

$$Ti_{(ox)}^{4+}HPO4^{2-} + OH^{-} \rightarrow Ti_{(ox)}^{4+}PO_{4(ads)}^{3-} + H_2O$$

The porous outer oxide layer can accommodate the adsorbed ions in the oxide film matrix and increase the biocompatibility of the implant material [21].

Table 1. Electrochemical impedance parameters for Ti-15Mo alloy in PBS solution at 37 ºC.

Time (h)	R_s $\Omega\,cm^2$	R_p $\Omega\,cm^2$	CPE_p $S_{cm}^{-2}(srad^{-1}n)$	n_p	R_b $\Omega\,cm^2$	CPE_b $S_{cm}^{-2}(srad^{-1}n)$	n_b	$W_b(R)$ $\Omega\,cm^2$	$W_b(T)$ s	$W_b(P)$	χ^2
2	2.21	1294	$2.52x10^{-5}$	0.93	31259	$4.68x10^{-5}$	0.58	13314	28.2	0.58	$9.96x10^{-5}$
24	3.26	519.3	$2.48x10^{-5}$	0.93	32698	$4.47x10^{-5}$	0.58	71019	2.28	0.58	$1.42x10^{-4}$
72	2.27	1375	$2.85x10^{-5}$	0.92	32394	$5.51x10^{-5}$	0.62	2765	29.5	0.76	$3.73x10^{-4}$
120	2.98	1503	$3.10x10^{-5}$	0.91	24138	$6.60x10^{-5}$	0.60	3570	31.6	0.71	$3.96x10^{-4}$
168	3.29	1433	$2.94x10^{-5}$	0.92	21781	$5.80x10^{-5}$	0.62	5809	34.5	0.65	$2.95x10^{-4}$
240	1.61	918.0	$2.80x10^{-5}$	0.93	16738	$6.44x10^{-5}$	0.59	5180	33.3	0.64	$2.85x10^{-4}$
360	2.74	1134	$3.18x10^{-5}$	0.92	15147	$6.91x10^{-5}$	0.63	5944	45.2	0.62	$2.39x10^{-4}$

The changes in phase angles, impedance modulus and semicircle size in Figs. 3 and 4 also show such changes. In the low frequency range in Fig. 3, where the barrier layer plays a role, it can be clearly seen that the phase angle increases up to 24 hours after which it slowly decreases till 360 hours. Similarly, in the low frequency range, the impedance modulus increases up to 24 hours and then drops till 360 hours. The diameter of the semicircle also seems to increase up to 24 hours and then a decrease is seen up to 360 hours. The initial increase in the barrier layer resistance accounts for the growth of the oxide in solution and the slow decrease afterwards is due to the attack by chloride ions from the saline solution.

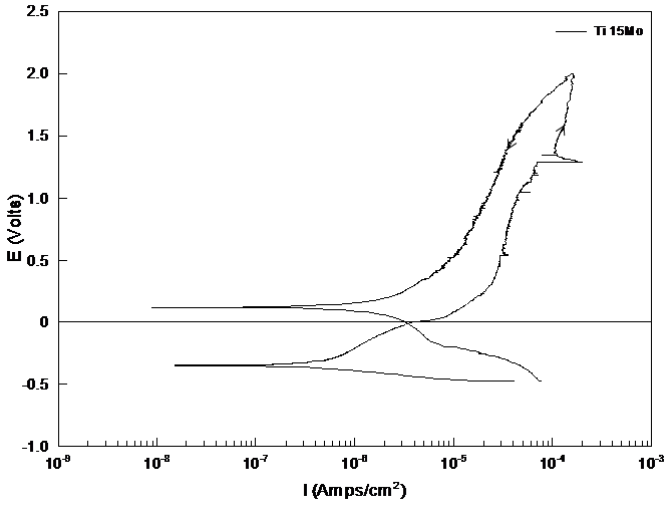

Figure 5. Cyclic potentiodynamic polarization curve for Ti-15Mo alloy in PBS solution at 37 ºC.

Fig 5 shows the cyclic polarization curve for Ti-15Mo alloy in PBS solution at 37 ºC and Table 2 shows the corrosion parameters evaluated from the curve. The E_{corr} of the reverse scan is more positive than the E_{corr} of the forward scan, which

further indicates the resistance to pitting and shows the formation of a stable oxide film during the forward scan [26].

Table 2. Corrosion parameters for Ti-15Mo alloy in PBS solution at 37 ºC.

Alloy	$-\beta_c$ ($Vdecade^{-1}$)	β_a ($Vdecade^{-1}$)	E_{corr} (F.S.) (V)	E_{corr} (R.S.) (V)	I_{corr} (μAcm^{-2})	E_{pass} (V)	I_{pass} (μAcm^{-2})
Ti15Mo	0.081	0.346	-0.349	0.121	0.3446	0.303	23.578

Conclusions

1. A two time constant model for the Bode and the Nyquist impedance plots, of a duplex oxide layer has been found to be an acceptable circuit to model Ti-15Mo alloy-solution interface.
2. The initial increase in the barrier layer resistance accounts for the growth of the oxide in solution and the slow decrease afterwards is due to the attack by chloride ions from the saline solution.
3. The porous outer oxide layer can accommodate the adsorbed ions in the oxide film matrix and aid in increasing the biocompatibility of the implant material.
4. The barrier layer resistance is an order of magnitude higher than the porous layer resistance.
5. Ti-15Mo alloy shows a tendency to resist localized corrosion.

References

1. J. Lemons, R. Venugopalan, L. Lucas, in Corrosion and Biodegradation; A. Von Recum, ed., Taylor Francis Inc: New York, 1999, 155-167.
2. K. Wang, *Materials Science and Engineering A* 213 (1996) 134-137. 10.1016/0921-5093(96)10243-4
3. M.F. Lopez, J.A. Jimenez, A. Gutierrez, *Electrochimica Acta* 48 (2003) 1395-1401. 10.1016/S0013-4686(03)00006-9
4. I. Milosev, M. Metikos-Hukovic, H. H. Strehblow, *Biomaterials* 21 (2000) 2103-2113. 10.1016/S0142-9612(00)00145-9
5. S. Rao, T. Ushida, T. Tateishi, Y. Okazaki, S. Asao, *Bio-Medical Materials Engineering* 6 (1996) 79-86.
6. P.R. Walker, J. Leblanc, M. Sikorska, *Biochemistry* 28 (1990) 3911-3915. 10.1021/bi00435a043
7. S. Yumoto, H. Ohashi, H. Nagai, S. Kakimi, Y. Ogawa, Y. Iwata, *International Journal of PIXE* 2 (1992) 493-504. 10.1142/S0129083592000531
8. R. Banerjee, S. Nag, J. Stechschulte, H.L. Fraser, *Biomaterials* 25 (2004) 3413-3419. 10.1016/j.biomaterials.2003.10.041
9. S. Nag, R. Banerjee, J. Stechschulte, H.L. Fraser, *J. Mater. Sci.: Mater Med.* 16 (2005) 679-685. 10.1007/s10856-005-2540-6

10. S. Nag, R. Banerjee, H. L. Fraser, *Materials Science and Engineering C* 25 (2005) 357-362. 10.1016/j.msec.2004.12.013
11. D.M. Brunette, P. Tengvall, M. Textor, P. Thomsen, Titanium in Medicine: Material Science, Surface Science, Engineering, Biological Responses and Medical Applications, Springer, 2001.
12. M. Karthega, V. Raman, N. Rajendran, *Acta Biomaterialia* 3 (2007) 1019-1023. 10.1016/j.actbio.2007.02.009
13. C. Lavos-Valereto, S. Wolynec, I. Ramires, A.C. Guastaldi, I. Costa, *J. Mater. Sci: Mater. Med.* 15 (2004) 55-59. 10.1023/B:JMSM.0000010097.86245.74
14. V.R. Jablokov, M.J. Nutt, M.E. Richelsoph, H.L. Freese, *J. of ASTM International* 2(8) (2005) 83-100, Article ID JAI13033. 10.1520/JAI13033
15. L.D. Zardiackas, D.W. Mitchell, J.A. Disegi, ASTM STP1272, ASTM International, West Conshohocken, PA, 1996, 60-75.
16. J. Bogan, L. Zardiackas, J. Disegi, Transactions, 27th Annual Meeting of the society of Biomaterials, St. Paul. MN, April 24-29, 2001.
17. J. Disegi, L. Zardiackas, Medical Device Materials, Proceedings from the Materials & Processes for Medical Devices Conference, 8-10 September, 2003, ASM International, Materials Park, OH, 2004, 337-342.
18. R.M. Davis, R.M. Forbes Jones, ASTM STP1272, ASTM International, West Conshohocken, PA, 1996, 17-29.
19. ASTM Standard F2066-08, ASTM International, Philadelphia, USA.
20. ASTM Standard F 2129-06, ASTM International, Philadelphia, USA.
21. W.A. Badawy, A.M. Fathi, R.M. El-Sherief, S.A. Fadl-Allah, *J. Alloys Compounds* 475 (2009) 911-916. 10.1016/j.jallcom.2008.08.061
22. J. Pan, D. Thierry, C. Leygraf, *Electrochimica Acta* 41 (1996) 1143-1153. 10.1016/0013-4686(95)00465-3
23. J.E.G. Gonzalez, J.C. Mirza-Rosca, *J. Electroanalytical Chem*. 471 (1999) 109-115. 10.1016/S0022-0728(99)00260-0
24. R. Vandenkerckhove, E. Temmerman, R. Verbeeck, *Mater. Sci. Forum* 289-292 (1998) 1289. 10.4028/www.scientific.net/MSF.289-292.1289
25. A.M. Al-Mayouf, A.A. Al-Swayih, N.A. Al-Mobarak, A.S. Al-Jabab, *Saudi Dental Journal* 14 (2002) 118-125.
26. R. Bhola, S.M. Bhola, B. Mishra, D.L. Olson, *Research Letters in Physical Chemistry* (2009) Article ID574359. 10.1155/2009/57435